

For submission to *Organic Geochemistry*

Impact of organic carbon reworking upon GDGT temperature proxies during the Paleocene-Eocene Thermal Maximum

Gordon N. Inglis[1]*, Pablo Martínez-Sosa [2,3], Jessica E. Tierney[2], Caitlyn R. Witkowski[4], Shelby Lyons[5,6], Allison A. Baczynski [5] and Katherine H. Freeman[5]

[1] *School of Ocean and Earth Science, University of Southampton, UK*

[2] *Department of Geosciences, University of Arizona, Tucson, AZ, USA*

[3] *Department of Earth Sciences, Utrecht University, Netherlands*

[4] *Organic Geochemistry Unit, School of Chemistry and School of Earth Science, University of Bristol, UK*

[5] *Department of Geosciences, Pennsylvania State University, University Park, PA, USA*

[6] *ExxonMobil, Houston, TX, USA*

* Corresponding author, email: Gordon.inglis@soton.ac.uk

Abstract

Glycerol dialkyl glycerol tetraethers (GDGTs) have been widely applied to coastal marine sediments to reconstruct past temperature variability. However, coastal environments are characterised by variability in the source, age and/or thermal maturity of different organic carbon (OC) pools and may bias various GDGT-based proxies. Here we analyse TEX_{86} and MBT_{5ME} values within a shallow marine sediment core (South Dover Bridge, Maryland) from the Paleocene-Eocene Thermal Maximum (PETM; 56 million years ago (Ma)) to explore how changes in OC reworking influence GDGT-derived sea surface and terrestrial temperature estimates, respectively. We demonstrate that TEX_{86} values are unaffected by an increase in soil- and fossil organic carbon during the PETM. In contrast, we find large and unexpected variations in MBT_{5ME}-derived temperature estimates (~6 to 25 °C) during the onset and core of the PETM at some sites. This coincides with input of reworked terrestrial OC from the Cenomanian-aged Raritan Formation. However, there is also an increase in the degree of cyclisation of tetramethylated branched GDGTs, suggesting that branched GDGTs are also derived from marine in-situ production. These factors preclude terrestrial temperature reconstructions at this site. We explored whether OC reworking is problematic in other PETM-aged coastal environments. Using GDGT metrics and the Branched and Isoprenoid GDGT Machine learning Classification algorithm (BIGMaC), we demonstrate that TEX_{86} values are mostly unaffected by changes in OC sources. However, MBT_{5ME} values are affected by marine and/or freshwater overprints, especially in environments with low terrestrial OC input. Taken together, this study highlights the importance of constraining the provenance of different GDGTs in marine and lacustrine environments.

Highlights:

- We assess the impact of organic carbon reworking on GDGT proxies during the PETM
- TEX_{86} values are unaffected by reworking and can be used to reconstruct SSTs
- MBT_{5ME} values can be highly variable and affected by multiple secondary inputs
- Discerning the provenance of GDGTs in coastal settings is crucial for related proxies

Keywords: GDGTs, biomarkers, hyperthermals, reworking

Introduction

The Paleocene-Eocene Thermal Maximum (PETM; 56 million years ago (Ma)) is the most abrupt carbon cycle perturbation of the last 66 million years (i.e., the Cenozoic) and is characterised by a negative carbon isotope excursion (~3-6‰; CIE) (Elling et al., 2019, McInerney & Wing 2011). The CIE is accompanied by a ~4 to 6 °C increase in global mean surface temperatures (Dunkley-Jones et al., 2013, Inglis et al., 2020, Tierney et al., 2022). However, despite evidence for warming in different regions, especially the SW Pacific (Inglis et al., 2021, Sluijs et al., 2011), mid-latitude Atlantic Ocean (Sluijs et al., 2007, Sluijs et al., 2014, Zachos et al., 2006), and Arctic Ocean (Sluijs et al., 2006, Weijers et al., 2007a), the spatial and temporal patterns of warming remain poorly constrained. This is mostly due to sparse data coverage and/or proxy-related uncertainties (Hollis et al., 2019).

The TEX_{86} proxy (Schouten et al., 2002) is based on the distribution of isoprenoidal glycerol dialkyl glycerol tetraethers (isoGDGTs) and has been widely applied to coastal marine sediments to reconstruct sea surface temperature (SST) change during the PETM (Frieling et al., 2017, Sluijs et al., 2011, Sluijs et al., 2006, Sluijs et al., 2014, Stokke et al., 2020). IsoGDGTs are synthesised by archaea and comprised of two isoprenoid side chains containing up to eight cyclopentane moieties (although rarely more than 4 cyclopentane moieties; Schouten et al., 2013 and ref. therein). The number of cyclopentane moieties increases at higher temperatures (De Rosa et al., 1980, Uda et al., 2004) and yields a more densely packed membrane. In the marine realm, isoGDGTs are mainly derived from marine Thaumarchaeota living within the upper 50-300 m of the water column (Church et al., 2010, Rattanasriampaipong et al., 2022). However, the input of isoGDGTs from the terrestrial biosphere could complicate TEX_{86} values during the PETM. The input of soil-derived isoGDGTs into the marine realm (Weijers et al., 2006) can be assessed using the branched-to-isoprenoidal tetraether (BIT) index (Hopmans et al., 2004). Previous work indicates that

TEX_{86} estimates with BIT values > 0.4 should not be used for SST reconstruction (Weijers et al., 2006), but it is unclear whether this threshold is globally applicable in marine and lacustrine sediments (Inglis et al., 2015). Erosion and lateral transport of isoGDGTs from exhumed ancient sedimentary rocks (i.e. petrogenic OC; OC_{petro}) may also affect TEX_{86}-based SST estimates. Any potential impact will depend strongly on the distribution of GDGTs in the original source material. However, the impact of thermal maturation itself can also be substantial. For example, in an artificial maturation experiment, TEX_{86} values decrease from ~0.65 to 0.40 in response to increasing burial temperatures. Subsequently, input of OC_{petro} could lead to lower-than-expected TEX_{86} values (Schouten et al., 2004). Input of OC_{petro} will also influence the carbon isotopic composition ($\delta^{13}C$) of isoGDGTs (Pearson et al., 2016), potentially impacting archaeal lipid-derived pCO_2 proxy estimates (Hurley et al., 2019, Pearson et al., 2019).

The MBT_{5ME} proxy (De Jonge et al., 2014a, Weijers et al., 2007b) is based on the distribution of branched GDGTs and has been applied to coastal marine sediments to reconstruct mean annual air temperature (MAAT) changes during the PETM (Bijl et al., 2013, Inglis et al., 2021, Sluijs et al., 2020). Branched GDGTs are synthesised by (acido)bacteria (Chen et al., 2022, Halamka et al., 2023) and comprised of two *n*-alkyl chains, each containing 4-6 methyl groups and 0-2 cyclopentane moieties (Schouten et al., 2013). The number of methyl groups varies as a function of temperature and is the premise of the MBT_{5ME} mean air temperature (MAT) proxy (De Jonge et al., 2014b). The MBT_{5ME} proxy assumes that brGDGTs are sourced from soil OC. However, the input of brGDGTs from rivers and/or alkaline soils can lead to lower reconstructed MAAT estimates (Crampton-Flood et al., 2021, Warden et al., 2016). A higher abundance of 6-methyl brGDGT isomers in alkaline environments and can overprint MBT_{5ME} values, especially in areas with substantial fluvial discharge. Branched GDGTs can also be produced in the marine water column (Liu et al,. 2014; Xie et al,. 2014;

Xiao et al., 2016) and marine sediments (Crampton-Flood et al., 2019). The distribution of marine-produced brGDGTs is distinct from other environments and is characterised by: (i) a higher relative proportion of cyclopentane rings in tetramethylated brGDGTs (Sinninghe Damsté 2016) and (ii) a higher relative proportion of hexa- to pentamethylated GDGTs (Xiao et al,. 2016). Both are consistent with production in a relatively alkaline environment. Input of marine-derived brGDGTs may impact MBT_{5ME}-temperature estimates in coastal environments (Crampton-Flood et al., 2021, Sinninghe Damsté 2016) but can be partially resolved by screening and excluding samples and/or correcting for possible marine/riverine overprints (Crampton-Flood et al., 2018) using a mixing model approach based on global soil and coastal marine calibration datasets (Crampton-Flood et al., 2018). However, the approach is not suitable for sites with low terrestrial OC input (Crampton-Flood et al., 2018). The input of brGDGTs from sedimentary rocks (e.g., paleosols, coal) may also affect MBT_{5ME} estimates, although the impact is unclear (Schouten et al., 2013).

Here, we evaluate how changes in the source, age and/or thermal maturity of different organic carbon (OC) pools affect GDGT-based proxies during the PETM. We focus on sediments from a shallow marine (< 150 m water depth) sediment core on the Atlantic Coastal Plain (South Dover Bridge, Maryland). The selected site features delivery of both biospheric and petrogenic OC during the core of the PETM (Lyons et al., 2018) and is therefore an ideal natural laboratory. We use various GDGT-based screening metrics alongside a new machine learning-based approach to evaluate how changes in OC reworking affect MBT_{5ME} and TEX_{86} values at this site. Using a similar approach, we also assess the impact of OC reworking in other PETM-aged shallow marine environments to understand the fidelity of GDGT-based temperature estimates during abrupt climate change events.

Methods

Site description

South Dover Bridge (SDB; Fig. 1) is located near the Salisbury Embayment on the Atlantic Coastal Plain. The site was drilled by the United States Geological Survey (USGS) in Talbot County, Maryland (González et al., 2012). SDB captures the pre-onset excursion (POE; ~205 to 207 m), a short-lived warming event that precedes the onset of the PETM, and the onset and core of the PETM (~188 to 204 m) (Babila et al., 2022, Self- Trail et al., 2017). High sedimentation rates (from ~1 to 16 cm kyr^{-1}) in a shallow water (>150 m) setting characterize the sample site (Doubrawa et al., 2022). Most PETM-aged sites exhibit a negative carbon isotope excursion define the onset and core of the PETM (see Wing and McInenery 2013 and ref. therein). At SDB, the carbon isotopic composition ($\delta^{13}C$) of carbonate and bulk organic matter initially decreases by 4‰ and 3.5‰, respectively. However, bulk organic matter $\delta^{13}C$ values increase by ~6‰ within the PETM core and recovery (Lyons et al., 2019). This is associated with an increase in hopane thermal maturity ratios (i.e., T_s/T_s+T_m [up to 0.86], C_{31}-homohopane 22S/(22S+22R) [up to 0.53], and norhopane/hopane [up to ~2.6]; Lyons et al., 2018). This indicates the input of ^{13}C-enriched recycled petrogenic OC, likely weathered from Cenomanian deltaic sands and shales of the Raritan facies of the upper Potomac Formation (Lyons et al, 2019). The core of the PETM also coincides with: i) an increase in total organic carbon (TOC) content from ~0.15 to ~0.45 wt. % (Lyons et al., 2019; Supplementary Information) and ii) input of terrestrial organic matter (inferred via an increase in the terrestrial-aquatic ratio [TAR]) (Lyons et al., 2019).

Analytical methods

Approximately 15 g of sediment from 36 samples was extracted using accelerated solvent extraction (ASE) at Pennsylvania State University (see Lyons et al., 2018). The total lipid extract (TLE) was subsequently dried under a stream of nitrogen (N_2) and separated into different compound classes (aliphatic, aromatic and polar) using silica column chromatography and mobile phases of 100% hexane (aliphatic fraction), 90% hexane:10% methylene chloride (aromatic fraction) and 70% methylene chloride:30% methanol (*v*/*v*) (polar fraction). The polar fraction was dissolved in hexane:isopropanol (99:1 *v*/*v*), passed through 0.45 µm PTFE (polytetrafluoroethylene) filters and analysed by high-performance liquid chromatography / atmospheric-pressure chemical ionization–mass spectrometry (HPLC/APCI-MS) at the University of Bristol following the methods of Hopmans et al. (2016).

GDGT proxies

The TEX_{86} index is defined as follows (Schouten et al, 2002):

$$TEX_{86} = GDGT\text{-}2 + GDGT\text{-}3 + Cren' / GDGT\text{-}1 + GDGT\text{-}2 + GDGT\text{-}3 + Cren' \qquad \text{(eq. 1)}$$

Where numbers refer to GDGT structures (Fig. S1). TEX_{86} is converted to sea surface temperature (SST) using the Bayesian calibration model BAYSPAR (Tierney & Tingley, 2014) with a prior mean of 25 °C and prior standard deviation of 15 °C.

The Ring Index (RI) represents the weighted average of cyclopentane moieties in GDGT compounds (Zhang et al., 2016):

$$\text{Ring Index} = (GDGT\text{-}0 * 0) + (GDGT\text{-}1 * 1) + (GDGT\text{-}2 * 2) + (GDGT\text{-}3 * 3) + (Cren * 4) + (Cren' * 4) \qquad \text{(eq.2)}$$

This metric helps to quantify the extent to which samples deviate from the modern TEX_{86}-RI relationship (ΔRI). Zhang et al. (2016) argue that samples with ΔRI values > 0.3 indicate potentially problematic TEX_{86} values.

The Methane Index (MI) is used to constrain the impact of anaerobic methanotrophy upon TEX_{86} values (Zhang et al., 2011):

Methane Index = (GDGT-1 + GDGT-2 + GDGT-3) / (GDGT-1 + GDGT-2 + GDGT-3 + Cren. + Cren') (eq.3)

Low MI values (<0.3) indicate normal, marine conditions and high values (>0.5) indicate high rates of AOM.

The MBT_{5ME} index is defined as follows (De Jonge et al., 2014):

MBT_{5ME} = Ia + Ib + Ic / Ia + Ib + Ic + IIa + IIa' + IIb + IIb' + IIc + IIc' + IIIa + IIIa' (eq. 4)

Numbers refer to GDGT structures (Fig. S2). MBT_{5ME} is converted to mean annual air temperature (MAAT) using a Bayesian calibration model $BAYMBT_0$ (Crampton-Flood et al., 2020) with a prior mean of 25 °C and prior standard deviation of 15 °C.

In addition to temperature, the distribution of brGDGTs can also be influenced by pH. This is captured by a modified version of the cyclisation of branched tetraethers (CBT) index (Weijers et al., 2007) and is defined as follows (De Jonge et al,. 2014):

CBT' = ^{10}log (Ic + IIa' + IIb' + IIc' + IIIa' + IIIb' + IIIc) / (Ia + IIa + IIIa) (eq. 5)

$$pH = 7.15 + 1.59 * CBT' \qquad \text{(eq. 6)}$$

The Branched vs. Isoprenoidal Tetraether (BIT) index captures the relative input of terrestrial versus marine OC matter and is defined as follows (Hopmans et al,. 2004):

$$BIT = (Ia+IIa+IIa'+IIIa+IIIa') / (Ia+IIa+IIa'+IIIa+IIIa'+Crenarchaeol) \qquad \text{(eq.7)}$$

This includes the 5-methyl (i.e. IIa) and 6-methyl (i.e. IIa') brGDGTs that were previously analysed as co-eluting compounds by Hopmans et al, (2004). Weijers et al. (2006) argue that TEX_{86} values with BIT values > 0.4 should not be used for SST reconstruction.

The degree of cyclisation of tetramethylated brGDGTs ($\#rings_{tetra}$) is used to assess input of brGDGTs from marine environments and is defined as follows (Sinninghe Damsté 2016):

$$\#rings_{tetra} = (Ib + 2 * Ic) / (Ia + Ib + Ic) \qquad \text{(eq.8)}$$

High $\#rings_{tetra}$ values (> 0.7) are interpreted to represent in-situ marine production. The ratio of 5- to 6-methyl brGDGTs is also used to detect input from alkaline marine environments. This is represented by the isomer ratio (IR) (De Jonge et al., 2015, De Jonge et al., 2014c):

$$IR = (IIa' + IIb' + IIc' + IIIa' + IIIb' + IIIc') / (IIa + IIa' + IIb + IIb' + IIc + IIc' + IIIa + IIIa' + IIIb + IIIb' + IIIc + IIIc') \qquad \text{(eq. 9)}$$

Machine learning analysis

Samples are assigned into likely depositional environments using the Branched and Isoprenoid Machine learning Classification (BIGMaC) algorithm. BIGMaC is a Random Forest algorithm trained with branched and isoprenoidal GDGT data from 1153 samples from lake (162), marine (215), peat (475), river (105), and soil samples (196) (Martínez-Sosa et al., 2023). Briefly, this algorithm was developed by classifying the samples from the dataset into discrete clusters, named *Lake-type*, *Marine-type*, *Peat-type*, and *Soil-type* (which contains both river and soil samples). Four classification methods were compared (Random Forest, XGBoost, K-nearest neighbour, and Naïve Bayes), and the best performing one, Random Forest, was selected according to its recall and precision metric (F1=0.95). The model was trained only on modern samples, but has been shown to perform well in Eocene-aged sediments (Martinez-Sosa et al., 2023).

In order to apply BIGMaC, the fractional abundance of each GDGT was calculated with respect to the total sum of GDGTs (branched + isoprenoidal) for all the samples (**Fig. 2**). The trained algorithm was then applied to the modified dataset using the predict() function from the stats R package (R core team, 2022). We assess the composition of each dataset using Principal Component Analysis (PCA) using the prcomp from the stats package (R core team, 2022) and the default parameters. The data analytical approach allowed us to compare and visualize the complete GDGT profile of all samples.

Results

GDGT distributions

The isoprenoidal GDGT (isoGDGT) distribution during the latest Paleocene (~ 209 to 204 m) is dominated by crenarchaeol (> 50% of the isoGDGT assemblage). The relative abundance of isoGDGT-0, -1 and -2 decreases during the core of the PETM (~204 to 188 m) whereas the relative abundance of crenarchaeol and its regioisomer increase. The branched GDGT (brGDGT) distribution during the latest Paleocene (~ 209 to 204 m) is dominated by brGDGT-Ia (~45% of the brGDGT assemblage). The relative abundance of brGDGT-IIa and –IIIa is low (~7 and 4% of the brGDGT assemblage, respectively). During the PETM, the relative abundance of brGDGT-Ia exhibits a wide range (~30% to ~60% of the total brGDGT assemblage) and there is a relative increase in brGDGT-Ic (up to ~25% of the total brGDGT assemblage), brGDGT-IIa (up to ~30% of the total brGDGT assemblage) and brGDGT-IIIa (up to ~15% of the total brGDGT assemblage).

The BIGMaC algorithm classifies the GDGT assemblage into either marine-type distributions (n = 34) or soil-type distributions (n = 2) (Fig. 2a). The samples that are classified as soil-type coincide with the lowest MBT_{5ME} values (Fig. 3) and contain a higher abundance of brGDGTs versus isoGDGTs compared to other samples. PCA was performed to: (i) elucidate differences in GDGT distributions, and (ii) determine the importance of individual GDGTs in determining clustering (Fig. 2a). Our results indicate that the first two principal components explain >90% of the variance in the data. The first principal component (PC1) accounts for 66% of the variance, and the second component (PC2) accounts for 25%. PCA separates the marine- and soil-type distributions into distinct clusters (Fig. 2a).

GDGT-based temperature and pH estimates

During the latest Paleocene (~ 209 to 204 m), TEX_{86} values are stable (average 0.69 ± 0.02; n = 14). TEX_{86} values do not vary throughout the pre-onset excursion (POE) (c.f. Babila et al., 2022) and increase (up to 0.90) during the onset of the PETM (~ 204 m; Fig. 3a), corresponding to ~10°C of surface ocean warming (Fig. 4c). TEX_{86} values remain high during the PETM core (0.87 ± 0.04; ~ 204 to 188 m) and gradually return to pre-PETM values during the PETM recovery (0.72) (Fig. 3a).

During the latest Paleocene (~209 to 204 m), MBT_{5ME} values are relatively stable (average 0.83 ± 0.06) (Fig. 3b). MBT_{5ME}-derived MAAT estimates range from 16 to ~22°C (Fig. 5c). MBT_{5ME} values exhibit large fluctuations during the PETM (~204 to 188 m; Fig. 5b) and MBT_{5ME}-derived MAAT estimates range from 9 to ~25°C (Fig. 5c). During the latest Paleocene (209 to 204 m), the IR is stable and high (0.51 ± 0.07) and declines during the PETM (0.28 ± 0.11) (Fig. 5e). The $\#rings_{tetra}$ values increase between the latest Paleocene (~0.4) and the PETM core (~0.6 to 0.7) with a gradual decline during the PETM recovery to pre-event values (~0.4) (Fig. 5d). BIT values span a wide range (0.15 to 0.70) and suggest variable terrestrial input during the latest Paleocene and PETM (Fig. 3d).

Discussion

Soil or peat input has minimal impact on TEX_{86} values during the PETM

The input of terrestrial-derived isoGDGTs from soil and/or peat can complicate TEX_{86} estimates in marine sediments (Weijers et al., 2006). Previous work indicates that TEX_{86} estimates with BIT values > 0.4 should not be used for SST reconstruction (Weijers et al., 2006). However, application of the suggested cut-off depends on the nature of the source catchment (see Inglis et al, 2015 and discussion therein) and the threshold for excluding TEX_{86} values (i.e., BIT > 0.4; Weijers et al., 2006) is often higher in marine settings (Douglas et al., 2014, Inglis & Tierney 2020). At SDB, there are multiple lines of evidence for enhanced terrigenous input during the PETM (relative to the latest Paleocene), including: i) higher sedimentation rates (an increase from ~2.4 to >20 cm/kyr) (Doubrawa et al., 2019, Robinson & Spivey 2019), ii) an increase in contemporaneous and/or reworked terrestrial leaf wax biomarkers (Lyons et al., 2019), and iii) an increase in biogenic magnetic particles (Kopp et al., 2009). Subsequently, the input of terrestrial-derived isoGDGTs may affect TEX_{86} estimates.

To explore whether input of terrestrial-derived isoGDGTs affects TEX_{86} estimates further, we use the BIT index to constrain the relative input of soil- and peat-derived OC into the marine realm. Prior to the PETM, the BIT index is relatively constant and ranges between 0.2 and 0.3. These low values suggest minimal soil- or peat-derived OC input into the marine realm. During the PETM, the BIT index exhibits considerable variability and fluctuates from ~0.15 (marine-dominated OC) to ~0.65 (soil- or peat-dominated OC). Fluctuating and highly variable values indicate episodic delivery of soil- and/or peat-derived OC into the marine realm, consistent with model evidence for an increase in extreme rainfall events during the PETM within this region (Rush et al., 2021, Rush et al., 2023). We note that the BIT index has previously been shown to be controlled strongly by crenarchaeol (rather than brGDGT) concentrations (Smith et al., 2012). As such, brGDGT concentrations (rather than the BIT index) may be a more robust tracer for soil OC (Fietz et al., 2011, Smith et al., 2012). Despite this caveat, an increase in terrigenous OM (inferred via BIT indices) is consistent with elevated terrestrial-aquatic ratios (TAR; Lyons et al., 2019), although it is unclear whether long-chain *n*-alkanes are penecontemporaneous or reworked (Lyons et al., 2019).

Crucially, samples with high BIT values (>0.4) do not yield significantly different (<1.5 °C) TEX_{86}-inferred temperature estimates than samples with lower BIT values (<0.4). Therefore, the threshold for excluding TEX_{86} values because of soil OC input is likely to be higher than 0.4 at SDB. Indeed, the BIGMaC algorithm classifies only two samples as “soil” derived (195.07 and 186.6 m). These samples have the highest BIT indices (0.61 and 0.65, respectively). We note that PETM samples contain a higher abundance of crenarchaeol compared to the pre-PETM and may bias classification towards a marine source. To explore this further, we examined the sensitivity of the model to changes in crenarchaeol alone (Figure S3) by setting the peak area of crenarchaeol to pre-onset levels (~0.55, compared with the >0.7 from PETM). The revised classification results show that most samples preserve the original classifications. The only exception are two additional samples that are now classified as “Soil-type” (~11% of samples; Figure S3). These samples have a relatively high abundance of brGDGT-IIa’ and a relatively low abundance of crenarcheol isomer. Thus, we conclude that while samples are sensitive to the increase in crenarchaeol during the PETM, the classification is not determined by this compound alone (see also Martinez-Sosa et al,. 2023) and argue that samples with BIT indices up to 0.6 can be used to reconstruct SST at SDB.

We also (re)investigated the input of soil- and peat-derived OC into the marine realm at other PETM-aged sites. Previous work from PETM-aged samples at IODP Site 302 (Lomonosov Ridge; ~390 to 368 mbsf) suggests that many samples are characterised by enhanced input of soil- and peat-derived OC. For example, 38 out of 124 samples yield high BIT indices (> 0.4) and 37 out of 124 samples yield high ΔRIs (>0.3) (Appendix). Yet, BIGMaC classifies only two samples as “soil” derived (2% of total samples) (Fig. 2d) and only three samples as “peat derived” (3% of samples). The “peat-type” samples are associated with intermediate BIT indices (~0.4) and do not form a distinct cluster in our PCA (Fig. 2d). We argue that these “peat” samples can be used to reconstruct SST at this site. However, PCA classifies the “soil” samples into a distinct cluster (Fig. 2d), indicating that these samples are overprinted by terrestrial input and should be excluded (c.f. South Dover Bridge). Crucially, the “soil” impacted samples (371.2 and 371.4 m) are associated with very high BIT indices (>0.7), again suggesting that the threshold for excluding TEX_{86} values due to soil input is higher than defined in previous studies (i.e., >0.4 for BIT and >0.3 for ΔRIs; see Weijers et al., 2006; Zhang et al., 2015).

At Otaio River (New Zealand) (Inglis et al., 2021), BIGMaC classified sixteen samples as “peat” derived (67% of total samples) and four samples as “soil” derived (17% of total samples) (Fig. 2c). The “peat” and “soil” samples are characterised by very high BIT values (>0.8) and high Methane Indices (average: 0.76), both of which are consistent with sedimentological evidence for deposition in a methane-rich wetland environment or low-energy deltaic setting (Inglis et al., 2021). This finding highlights the utility of BIGMaC as a tool to distinguish changes in the depositional environment (e.g., terrestrial versus marine). Two samples with moderate BIT indices (0.62 and 0.56, respectively) are assigned as "marine-type" distributions and form a distinct "marine" cluster (Fig. 2c). These samples are associated with increasing marine influence at this site (Inglis et al., 2021) and are not associated with other secondary overprints (e.g., MI < 0.2, ΔRI < 0.3). This implies that TEX_{86} values can be used to reconstruct SST at this site for these two samples (c.f. Inglis et al., 2021).

Finally, at ODP Site 1172 (SW Pacific) (Bijl et al., 2021, Sluijs et al., 2011), BIGMaC does not classify any samples as "soil" or "peat" derived (Fig. 2b). This is consistent with very low-to-moderate BIT indices (0.16 to 0.40) (Bijl et al., 2021) and low ΔRIs (<0.3). Subsequently, we conclude that TEX_{86} values are unaffected by terrestrial input at ODP Site 1172. Taken together, our results suggest that TEX_{86}-derived SST estimates at these location are unaffected by terrestrial input during the PETM, with the exception of samples with very high BIT values (typically > 0.6 and as high as 0.7). The lack of terrestrial input could be attributed to changes in sea level during the PETM. Rising sea levels have been documented in several mid- to-high latitude continental shelf sections during the PETM (e.g., Speijer and Morsi, 2002; Harding et al., 2011; Sluijs et al., 2014), including SDB (Doubrawa et al., 2022). Sea level rise would shift terrigenous OC deposition landwards and yield lower BIT indices (e.g., Sluijs et al., 2014). This may explain why TEX_{86}-derived SST estimates are largely unaffected by terrestrial input during the PETM.

Petrogenic OC input has variable impact on GDGT proxies during the PETM

South Dover Bridge is characterised by a positive carbon isotope excursion (CIE; ~6‰) in bulk OC (Lyons et al., 2019) and an increase in biomarker thermal maturity ratios (Lyons et al., 2019; Fig. 4e) during the core of the PETM (~192 to 202 m). This is attributed to enhanced delivery of thermally mature, ^{13}C-enriched OC into the marine shelf. The most likely source is the terrestrial-dominated Cenomanian-aged Raritan Formation (Lyons et al., 2019). Artificial maturation experiments (Schouten et al., 2004, Schouten et al., 2013) indicate that TEX_{86} and – to a lesser extent – MBT_{5ME} values decline at higher maturity. Therefore, the input of isoGDGTs and/or brGDGTs from thermally mature sedimentary rocks may lead to lower-than-expected TEX_{86} and MBT_{5ME} values during the core of the PETM. However, it will also be highly dependent upon the GDGT assemblage within the original source rock.

Hopane thermal maturity indicators can provide insights into the presence (Farrimond et al., 1998, Mackenzie et al., 1980) and/or proportion (Lyons et al, 2018) of OC derived from ancient sedimentary rocks (OC_{petro}). However, to differentiate between different source rocks (i.e., terrestrial vs marine), additional constraints are required (e.g., identification of reworked terrestrial or marine palynomorphs). Schouten et al. (2004) recommend excluding TEX_{86} and MBT_{5ME} values when 22S / (22S+22R) hopane ratios > 0.2 (Schouten et al., 2004). During the core of the PETM, 22S/(22S+22R) hopane ratios increase from ~0.1 (relatively immature) to ~0.5 (relatively mature) (Lyons et al,. 2019). These values are approaching equilibrium (~0.55-0.60; Farrimond et al., 1998) and correspond to an increase in the fraction of OC derived from thermally mature fossil sources (f_{fossil}; Fig. 4f). Intriguingly, this also coincides with increasing variability in MBT_{5ME} values (Fig. 5). Therefore, we suggest that brGDGTs could be derived from weathering of the nearby Raritan Formation. Samples of the Raritan Formation contain abundant leaves, pollen and amber deposits (Grimaldi et al., 2010) and were deposited in a deltaic environment. Samples also yield low HI indices (14-22) and high OI indices (48-79) (Lyons et al., 2019) and are characteristic of terrestrial OM (Lyons et al, 2019). As such, the input of pre-aged brGDGTs from the Raritan Formation could explain anomalous temperature estimates during the core of the PETM. It also implies that long-chain *n*-alkanes could be reworked from the Raritan Formation and may bias TAR values.

The input of thermally mature OC is predicted to bias TEX_{86} values. However, TEX_{86} values increase during the PETM as expected from other lines of evidence (Hollis et al., 2019). This implies that input of thermally mature OC does not affect TEX_{86} values in our setting. As 22S/(22S+22R) hopane ratios are approaching equilibrium values (up to 0.5), it is plausible that isoGDGTs in the original source rock have been completely degraded. This is consistent with Tibbett et al. (2022) who found that isoGDGT and brGDGT distributions were unaffected by reworking during the Eocene-Oligocene transition (~34 Ma), despite increased input of petrogenic OC (inferred via a decrease in *n*-alkane odd-over-even predominance ratios) (Tibbett et al., 2022). The impact of petrogenic OC in other PETM-aged sites is unclear because few studies report biomarker thermal maturity ratios. Thermal maturity indicators available from Otaio River indicate that the OC is thermally immature throughout the sample set (Inglis et al., 2021). However, we stress that elevated thermal maturity ratios are not necessarily a prerequisite for excluding TEX_{86} or MBT_{5ME} values. Instead, it will depend upon whether OC is allochthonous (Tibbett et al., 2022) or autochthonous.

Marine and freshwater input overprints MBT_{5ME} values during the PETM

At SDB, brGDGT-derived MAAT estimates from the pre-PETM interval indicate warm and stable terrestrial temperatures (ca. 20 to 22 °C; Fig. 5c). However, brGDGT-derived MAAT estimates exhibit a wide calculated temperature range (~6 to 25 °C) during the onset and core of the PETM (Fig. 5c). However palynological evidence suggests a gradual increase in terrestrial temperatures along the mid-Atlantic Coastal Plain (up to 4 °C) and limited variability within the body of the PETM (Willard et al., 2019). The contrast in temperature variability indicates additional controls on MBT_{5ME} values during the PETM.

The input of petrogenic OC from the Raritan Formation could explain anomalous temperatures during the core of the PETM (see above). However, the input of brGDGTs from rivers can also yield anomalously cold and/or variable temperature estimates (Crampton-Flood et al., 2018, Crampton-Flood et al., 2021, De Jonge et al., 2014c, Zell et al., 2014a, Zell et al., 2013). As rivers are typically characterised by a high relative proportion of 6-methyl brGDGTs compared to 5-methyl brGDGTs, riverine input can be recognised by higher IR ratios (typically >0.5) (De Jonge et al., 2015). However, IR values decrease at SDB during the PETM from ~0.5 to ~0.2 (Fig. 5e). These values are similar to modern soils (~0.1 to 0.2) (Crampton-Flood et al., 2020, De Jonge et al., 2014a) and suggest that brGDGTs are unlikely to be sourced from fluvial environments. This occurs despite evidence for the development of a large, river-dominated shelf during the PETM (i.e., the paleo-Potomac) (Kopp et al., 2009)

Branched GDGTs could be derived from older (i.e., pre-PETM) reworked soil deposits. The core of the PETM coincides with input of plant-derived organic matter (inferred via an order-of-magnitude increase in the terrestrial-aquatic ratio [TAR]). However, it is unclear whether long-chain *n*-alkanes are derived from penecontemporaneous soils or terrestrial organic carbon from the Cenomanian-aged Raritan Formation (Lyons et al., 2019). As reworking is a common feature in other mid-latitude PETM settings, such as the Gulf Coastal Plain (Sluijs et al., 2014), Austria (Hofmann et al., 2012), and northern Spain (Manners et al., 2013), we argue that both options are plausible. As there are large fluctuations in the TAR during the core of the PETM (ranging between ~10 to ~200; Fig. 4e), this implies major changes in OM sources and may explain why MBT_{5ME} values are so variable.

However, there is also growing evidence that brGDGTs are produced within the water column (Liu et al., 2014, Xie et al., 2014) and/or marine sediments (Crampton-Flood et al., 2019, Xiao et al., 2016). The source of branched GDGTs in the marine realm remains unknown, but their abundance within anoxic oxygen minimum zones (e.g,. Liu et al., 2014) implies an anaerobic source organism. Marine production can be assessed using the degree of cyclisation of tetramethylated brGDGTs (#rings$_{tetra}$), where values >0.7 indicate a definitive marine origin (Sinninghe Damsté 2016). At SDB, there is an increase in #rings$_{tetra}$ values during the PETM from ~0.3 to ~0.7 (Fig. 5d). These values are much higher than in modern soils (average 0.21 ± 0.19) and consistent with an increase in marine in-situ production. BIGMaC also classifies the majority of samples at SDB as "marine" derived (Fig. 2a). Crampton-Flood et al (2018) propose a method to remove the influence of marine production on MBT$_{5ME}$ values. However, the combination of low BIT values (0.1 to 0.3) and high #rings$_{tetra}$ values (up to 0.7) prevents any correction (see Crampton-Flood et al., 2018). In-situ marine production (inferred via high #rings$_{tetra}$ values) typically dominates within shallow water environments (~50 and 300 m water depth) (Sinninghe Damsté 2016). This is consistent with shallow water depths (<300m) at SDB during the PETM (Doubrawa et al., 2019, Self- Trail et al., 2017). Taken together, we argue that in-situ marine production – perhaps alongside input of thermally mature OC - explains variable MBT$_{5ME}$-derived temperature estimates during the core of the PETM.

We also assessed the potential impact of marine and/or fluvial overprints at other PETM-aged sites (Otaio River, New Zealand; ODP Site 1172, East Tasman Plateau; IODP Site 302, Lomonosov Ridge). At all three sites, #rings$_{tetra}$ values are consistently low (<0.3) and imply that marine in-situ production is unlikely to impact MBT$_{5ME}$ values. At Otaio River (Inglis et al., 2021) and IODP Site 302 (Sluijs et al., 2020), low IR values (0.1 to 0.3) indicate that input of brGDGTs from rivers is also minimal. In contrast, ODP Site 1172 exhibits relatively high IR values (average: 0.47; n = 26). This site notably lacks terrestrial warming during the PETM (Bijl et al., 2021, Sluijs et al., 2011), which could possibly be explained by the input of brGDGTs derived from arid and/or alkaline soils or rivers.

Intriguingly, the two PETM-aged sites that contain abnormal brGDGT distributions (ODP Site 1172 and SDB) also contain relatively low TOC values during the core of the PETM

(~0.5 and 0.6 wt. %, respectively. This is lower than Otaio River (> 1 to 60 wt. % TOC; Inglis et al., 2021) and IODP Site 302 (~2 wt. % TOC; Sluijs et al., 2006; Sluijs et al., 2021). Taken together, this implies that MBT_{5ME} values in coastal environments characterised by low terrestrial OC input are more likely to be affected by marine or freshwater overprints than sites with high terrestrial OC input (Zell et al., 2014a, Zell et al., 2014b).

Surface ocean warming in the Atlantic Coastal Plain during the PETM

Our results indicate that TEX_{86} values are unaffected by the input of reworked OC (see above) during the PETM. There is also no evidence for other additional controls on TEX_{86} values, such as input from methanogenic and/or methanotrophic Euryarchaeota (Figure S4). As a result, we can use TEX_{86} to reconstruct a continuous SST record in the Atlantic Coastal Plain during the PETM. Our results show that SST estimates increased between the latest Paleocene (average ~27 °C; 209 to 204 m depth) and PETM (average ~39 °C; 204-188 m depth) (Fig. 6b). The magnitude of warming between the pre-PETM and PETM (ΔSST = 12 °C) is similar to or higher than SSTs reconstructed from other sites on the Atlantic Coastal Plain, including Bass River (ΔSST = 5 to 8 °C) (Sluijs et al., 2007) and Wilson Lake (ΔSST = 9 to 11 °C) (Sluijs et al., 2007, Zachos et al., 2006). Our new results are also broadly consistent with TEX_{86}-inferred SST estimates from other PETM-aged mid-to-high latitude marginal marine sediments, including the East Tasman Plateau (~8 °C) (Sluijs et al., 2011), Western Siberian Seaway (~11°C) (Frieling et al., 2014), and Denmark (~7-10 °C) (Stokke et al., 2020).

However, the magnitude of warming inferred via TEX_{86} is far greater than that calculated via the Mg/Ca-based SST proxy from the same sediments (~3-4 °C; Babila et al., 2022; Fig. 6c-e) and at nearby sites (Bass River; ΔSST: ~3 °C) (Babila et al., 2016). It remains unclear why TEX_{86} yields a larger magnitude of warming compared to carbonate proxies during the PETM and other past warm climate intervals (Hollis et al., 2019). Although TEX_{86}

correlates strongly to SST or temperatures between 0 to 200 m water depth (Tierney and Tingley, 2014), Thaumarchaeota can live throughout the water column (Villanueva et al., 2015) and export of isoGDGTs from below the photic zone can influence TEX_{86} values, especially in deep-water (>1000m) environments (Rattanasriampaipong et al., 2022, Taylor et al., 2013). GDGT-2/GDGT-3 ratios can be used to evaluate deeper water column production; high values (typically >5) are indicative of deep-water production (Taylor et al., 2013). Our values are consistently low (ca. 2 to 3) and exhibit a thermal behaviour response (Rattanasriampaipong et al., 2022). Moreover, as SDB was deposited under shallow water depths (<150m) (Doubrawa et al., 2022), the impact of subsurface production is likely to be minor. Instead, some of these discrepancies might be attributed to uncertainties in TEX_{86}-derived SSTs in the upper temperature range (> 30 °C) (Inglis & Tierney 2020). However, there are also uncertainties regarding the depth habitat of surface-dwelling planktonic foraminifera during the PETM (e.g., *Acarinina* spp.) which may move deeper into the water column during the PETM, thus reducing the magnitude of estimated warming (Tierney et al., 2022).

Our new TEX_{86}-based SST estimates fail to capture the pre-onset excursion (POE) inferred via planktonic foraminifera Mg/Ca values (Fig. 6). However, the latter is based upon only two data points (Babila et al., 2022) and may not be representative. Our TEX_{86} record is instead consistent with the absence of cooling inferred via planktonic foraminifera $\delta^{18}O$ records (Babila et al., 2022). As Mg/Ca, $\delta^{18}O$ and TEX_{86} data from the POE remain at relatively coarse resolution (2, 5 and 4 samples within the POE, respectively), further work is required to determine the magnitude of warming and whether this was regionally and globally widespread.

Conclusions

Here we use sediments from South Dover Bridge (Maryland) to constrain the impact of organic carbon reworking on GDGT-based temperature estimates during the Paleocene-Eocene

Thermal Maximum (PETM). GDGT-based metrics and a novel machine learning algorithm indicates that TEX_{86} values are unaffected by input of biospheric and petrogenic OC during PETM. Therefore, TEX_{86} can be used to reconstruct a continuous SST record in the Atlantic Coastal Plain during the PETM. However, we find large and unexpected variations in MBT_{5ME}-derived mean annual air temperature estimates (~6 to 25 °C) during the onset and core of the PETM. This coincides with episodic delivery of biospheric and petrogenic terrestrial OC into the marine realm. It also coincides with an increase in the degree of cyclisation of tetramethylated branched GDGTs ($\#rings_{tetra}$ up to 0.7) and implies that branched GDGTs could also be derived from marine in-situ production. We find that marine and/or freshwater overprinting can be problematic in other PETM-aged sites, especially those characterised by low organic matter input. This suggests caution when applying brGDGT-based temperature proxies in shallow marine sediment cores with low terrestrial input.

Open Research

The GDGT fractional abundance data in the study are included in the supplementary information. V1.0 of the BIGMaC algorithm used for the classification of samples based on GDGT fractional abundances is preserved at 10.5281/zenodo.7513557 available via MIT license and developed openly in the tidymodels environment in R.

Acknowledgments

GNI is supported by a GCRF Royal Society Dorothy Hodgkin Fellowship (DHF\R1\191178) with additional support via the Royal Society (RF\ERE\231019, RF\ERE\210068). CRW is supported by Royal Society Dorothy Hodgkin Fellowship (DHF\R1\221014). We thank the National Environmental Isotope Facility (NEIF; No. NE/V003917/1) for analytical support. We acknowledge Jean Self-Trail (USGS) and the USGS Eastern Regional Drilling Crew who were influential in recovering the South Dover Bridge core. Finally, we thank Elizabeth Minor, the Associate Editor, and two anonymous reviewers whose thoughtful comments significantly improved the manuscript.

Conflict of Interest statement

The authors declare no conflicts of interest relevant to this study.

References

Babila TL, Penman DE, Standish CD, Doubrawa M, Bralower TJ, et al. 2022. Surface ocean warming and acidification driven by rapid carbon release precedes Paleocene-Eocene Thermal Maximum. *Science advances* 8: eabg1025

Babila TL, Rosenthal Y, Wright JD, Miller KG. 2016. A continental shelf perspective of ocean acidification and temperature evolution during the Paleocene-Eocene Thermal Maximum. *Geology* 44: 275-8

Bijl PK, Bendle JAP, Bohaty SM, Pross J, Schouten S, et al. 2013. Eocene cooling linked to early flow across the Tasmanian Gateway. *Proceedings of the National Academy of Sciences of the United States of America* 110: 9645

Bijl PK, Frieling J, Cramwinckel MJ, Boschman C, Sluijs A, Peterse F. 2021. Maastrichtian–Rupelian paleoclimates in the southwest Pacific–a critical re-evaluation of biomarker paleothermometry and dinoflagellate cyst paleoecology at Ocean Drilling Program Site 1172. *Climate of the Past* 17: 2393-425

Bottini C, Erba E, Tiraboschi D, Jenkyns H, Schouten S, Sinninghe Damsté J. 2015. Climate variability and ocean fertility during the Aptian Stage. *Climate of the Past* 11: 383-402

Chen Y, Zheng F, Yang H, Yang W, Wu R, et al. 2022. The production of diverse brGDGTs by an Acidobacterium providing a physiological basis for paleoclimate proxies. *Geochimica et Cosmochimica Acta* 337: 155-65

Church MJ, Wai B, Karl DM, DeLong EF. 2010. Abundances of crenarchaeal amoA genes and transcripts in the Pacific Ocean. *Environmental Microbiology* 12: 679-88

Crampton-Flood ED, Peterse F, Damsté JSS. 2019. Production of branched tetraethers in the marine realm: Svalbard fjord sediments revisited. *Organic Geochemistry* 138: 103907

Crampton-Flood ED, Peterse F, Munsterman D, Damsté JSS. 2018. Using tetraether lipids archived in North Sea Basin sediments to extract North Western European Pliocene continental air temperatures. *Earth and Planetary Science Letters* 490: 193-205

Crampton-Flood ED, Tierney JE, Peterse F, Kirkels FM, Damsté JSS. 2020. BayMBT: A Bayesian calibration model for branched glycerol dialkyl glycerol tetraethers in soils and peats. *Geochimica et Cosmochimica Acta* 268: 142-59

Crampton-Flood ED, van der Weijst CM, Van Der Molen G, Bouquet M, Yedema Y, et al. 2021. Identifying marine and freshwater overprints on soil-derived branched GDGT temperature signals in Pliocene Mississippi and Amazon River fan sediments. *Organic Geochemistry* 154: 104200

De Jonge C, Hopmans EC, Zell CI, Kim J-H, Schouten S, Damsté JSS. 2014a. Occurrence and abundance of 6-methyl branched glycerol dialkyl glycerol tetraethers in soils: Implications for palaeoclimate reconstruction. *Geochimica et Cosmochimica Acta* 141: 97-112

De Jonge C, Hopmans EC, Zell CI, Kim J-H, Schouten S, Sinninghe Damsté JS. 2014b. Occurrence and abundance of 6-methyl branched glycerol dialkyl glycerol tetraethers in soils: Implications for palaeoclimate reconstruction. *Geochimica et Cosmochimica Acta* 141: 97-112

De Jonge C, Stadnitskaia A, Fedotov A, Sinninghe Damsté JS. 2015. Impact of riverine suspended particulate matter on the branched glycerol dialkyl glycerol tetraether composition of lakes: The outflow of the Selenga River in Lake Baikal (Russia). *Organic Geochemistry* 83–84: 241-52

De Jonge C, Stadnitskaia A, Hopmans EC, Cherkashov G, Fedotov A, Sinninghe Damsté JS. 2014c. In situ produced branched glycerol dialkyl glycerol tetraethers in suspended particulate matter from the Yenisei River, Eastern Siberia. *Geochimica et Cosmochimica Acta* 125: 476-91

De Rosa M, Esposito E, Gambacorta A, Nicolaus B, Bu'Lock JD. 1980. Effects of temperature on ether lipid composition of Caldariella acidophila. *Phytochemistry* 19: 827-31

Doubrawa M, Stassen P, Robinson MM, Babila TL, Zachos JC, Speijer R. 2019. *New insights into shelf ecosystems prior and during the PETM*. Presented at Foram-Nanno 2019, Date: 2019/07/01-2019/07/04, Location: Fribourg, Switzerland

Doubrawa M, Stassen P, Robinson MM, Babila TL, Zachos JC, Speijer RP. 2022. Shelf Ecosystems Along the US Atlantic Coastal Plain Prior to and During the Paleocene-Eocene Thermal Maximum: Insights Into the Stratigraphic Architecture. *Paleoceanography and Paleoclimatology* 37: e2022PA004475

Douglas PMJ, Affek HP, Ivany LC, Houben AJP, Sijp WP, et al. 2014. Pronounced zonal heterogeneity in Eocene southern high-latitude sea surface temperatures. *Proceedings of the National Academy of Sciences*

Dunkley-Jones T, Lunt DJ, Schmidt DN, Ridgwell A, Sluijs A, et al. 2013. Climate model and proxy data constraints on ocean warming across the Paleocene–Eocene Thermal Maximum. *Earth-Science Reviews* 125: 123-45

Elling FJ, Gottschalk J, Doeana KD, Kusch S, Hurley SJ, Pearson A. 2019. Archaeal lipid biomarker constraints on the Paleocene-Eocene carbon isotope excursion. *Nature communications* 10: 1-10

Farrimond P, Taylor A, TelnÆs N. 1998. Biomarker maturity parameters: the role of generation and thermal degradation. *Organic Geochemistry* 29: 1181-97

Fietz S, Martínez- Garcia A, Huguet C, Rueda G, Rosell- Melé A. 2011. Constraints in the application of the Branched and Isoprenoid Tetraether index as a terrestrial input proxy. *Journal of Geophysical Research: Oceans* 116

Frieling J, Gebhardt H, Huber M, Adekeye OA, Akande SO, et al. 2017. Extreme warmth and heat-stressed plankton in the tropics during the Paleocene-Eocene Thermal Maximum. *Science advances* 3: e1600891

Frieling J, Iakovleva AI, Reichart G-J, Aleksandrova GN, Gnibidenko ZN, et al. 2014. Paleocene–Eocene warming and biotic response in the epicontinental West Siberian Sea. *Geology* 42: 767-70

González WA, Powars DS, Seefelt EL, Edwards LE, Self-Trail JM, et al. 2012. *Preliminary physical stratigraphy, biostratigraphy, and geophysical data of the USGS South Dover Bridge Core, Talbot County, Maryland. Rep. 2331-1258*, US Geological Survey

Grimaldi DA, Nascimbene PC, Penney D. 2010. Raritan (New Jersey) amber. *Biodiversity of fossils in amber from the major world deposits*: 167-91

Halamka TA, Raberg JH, McFarlin JM, Younkin AD, Mulligan C, et al. 2023. Production of diverse brGDGTs by Acidobacterium Solibacter usitatus in response to temperature, pH, and O2 provides a culturing perspective on br GDGT proxies and biosynthesis. *Geobiology* 21: 102-18

Hofmann C-C, Pancost R, Ottner F, Egger H, Taylor K, et al. 2012. Palynology, biomarker assemblages and clay mineralo-gy of the Early Eocene Climate Optimum (EECO) in the transgressive Krappfeld succession (Eastern Alps, Austria). *Austrian Journal of Earth Sciences* 105

Hollis CJ, Dunkley Jones T, Anagnostou E, Bijl PK, Cramwinckel MJ, et al. 2019. The DeepMIP contribution to PMIP4: methodologies for selection, compilation and analysis of latest Paleocene and early Eocene climate proxy data, incorporating version 0.1 of the DeepMIP database. *Geoscientific Model Development* 12: 3149-206

Hopmans EC, Schouten S, Damsté JSS. 2016. The effect of improved chromatography on GDGT-based palaeoproxies. *Organic Geochemistry* 93: 1-6

Hopmans EC, Weijers JW, Schefuß E, Herfort L, Sinninghe Damsté JS, Schouten S. 2004. A novel proxy for terrestrial organic matter in sediments based on branched and isoprenoid tetraether lipids. *Earth and Planetary Science Letters* 224: 107-16

Hurley SJ, Close HG, Elling FJ, Jasper CE, Gospodinova K, et al. 2019. CO2-dependent carbon isotope fractionation in Archaea, Part II: The marine water column. *Geochimica et Cosmochimica Acta* 261: 383-95

Inglis GN, Bragg F, Burls NJ, Cramwinckel MJ, Evans D, et al. 2020. Global mean surface temperature and climate sensitivity of the early Eocene Climatic Optimum (EECO), Paleocene–Eocene Thermal Maximum (PETM), and latest Paleocene. *Climate of the Past* 16: 1953-68

Inglis GN, Rohrssen M, Kennedy EM, Crouch EM, Raine JI, et al. 2021. Terrestrial methane cycle perturbations during the onset of the Paleocene-Eocene Thermal Maximum. *Geology* 49: 520-4

Inglis GN, Tierney JE. 2020. *The TEX86 Paleotemperature Proxy*: Cambridge University Press

Kopp RE, Schumann D, Raub TD, Powars DS, Godfrey LV, et al. 2009. An Appalachian Amazon? Magnetofossil evidence for the development of a tropical river- like system in the mid- Atlantic United States during the Paleocene- Eocene thermal maximum. *Paleoceanography* 24

Liu X-L, Zhu C, Wakeham SG, Hinrichs K-U. 2014. In situ production of branched glycerol dialkyl glycerol tetraethers in anoxic marine water columns. *Marine Chemistry* 166: 1-8

Lyons SL, Baczynski AA, Babila TL, Bralower TJ, Hajek EA, et al. 2019. Palaeocene–Eocene thermal maximum prolonged by fossil carbon oxidation. *Nature Geoscience* 12: 54-60

Mackenzie A, Patience R, Maxwell J, Vandenbroucke M, Durand B. 1980. Molecular parameters of maturation in the Toarcian shales, Paris Basin, France—I. Changes in the configurations of acyclic isoprenoid alkanes, steranes and triterpanes. *Geochimica et Cosmochimica Acta* 44: 1709-21

Manners HR, Grimes ST, Sutton PA, Domingo L, Leng MJ, et al. 2013. Magnitude and profile of organic carbon isotope records from the Paleocene–Eocene Thermal Maximum: Evidence from northern Spain. *Earth and Planetary Science Letters* 376: 220-30

Martínez-Sosa P, Tierney J, Perez-Angel LC, Stefanescu IC, Guo J, et al. 2023. Development and application of the Branched and Isoprenoid GDGT Machine learning Classification algorithm (BIGMaC) for paleoenvironmental reconstruction. *ESS Open Archive; 10.22541/essoar.167422960.07359877/v1*

McInerney FA, Wing SL. 2011. The Paleocene-Eocene Thermal Maximum: A perturbation of carbon cycle, climate, and biosphere with implications for the future. *Annual Review of Earth and Planetary Sciences* 39: 489-516

O'Brien CL, Robinson SA, Pancost RD, Damsté JSS, Schouten S, et al. 2017. Cretaceous sea-surface temperature evolution: Constraints from TEX 86 and planktonic foraminiferal oxygen isotopes. *Earth-Science Reviews*

Papadomanolaki NM, Sluijs A, Slomp CP. 2022. Eutrophication and deoxygenation forcing of marginal marine organic carbon burial during the PETM. *Paleoceanography and Paleoclimatology* 37: e2021PA004232

Pearson A, Hurley SJ, Elling FJ, Wilkes EB. 2019. CO2-dependent carbon isotope fractionation in Archaea, Part I: Modeling the 3HP/4HB pathway. *Geochimica et Cosmochimica Acta* 261: 368-82

Pearson A, Hurley SJ, Walter SRS, Kusch S, Lichtin S, Zhang YG. 2016. Stable carbon isotope ratios of intact GDGTs indicate heterogeneous sources to marine sediments. *Geochimica et Cosmochimica Acta* 181: 18-35

Rattanasriampaipong R, Zhang YG, Pearson A, Hedlund BP, Zhang S. 2022. Archaeal lipids trace ecology and evolution of marine ammonia-oxidizing archaea. *Proceedings of the National Academy of Sciences* 119: e2123193119

Robinson MM, Spivey WE. 2019. Environmental and geomorphological changes on the eastern North American continental shelf across the Paleocene- Eocene boundary. *Paleoceanography and Paleoclimatology* 34: 715-32

Rush WD, Kiehl JT, Shields CA, Zachos JC. 2021. Increased frequency of extreme precipitation events in the North Atlantic during the PETM: Observations and theory. *Palaeogeography, Palaeoclimatology, Palaeoecology* 568: 110289

Rush WD, Self-Trail J, Zhang Y, Sluijs A, Brinkhuis H, et al. 2023. Assessing Environmental Change Associated with Early Eocene Hyperthermals in the Atlantic Coastal Plain, USA. *EGUsphere*: 1-36

Schouten S, Hopmans EC, Schefuß E, Damste JSS. 2002. Distributional variations in marine crenarchaeotal membrane lipids: a new tool for reconstructing ancient sea water temperatures? *Earth and Planetary Science Letters* 204: 265-74

Schouten S, Hopmans EC, Sinninghe Damsté JS. 2004. The effect of maturity and depositional redox conditions on archaeal tetraether lipid palaeothermometry. *Organic Geochemistry* 35: 567-71

Schouten S, Hopmans EC, Sinninghe Damsté JS. 2013. The organic geochemistry of glycerol dialkyl glycerol tetraether lipids: a review. *Organic geochemistry* 54: 19-61

Self- Trail JM, Robinson MM, Bralower TJ, Sessa JA, Hajek EA, et al. 2017. Shallow marine response to global climate change during the Paleocene- Eocene Thermal Maximum, Salisbury Embayment, USA. *Paleoceanography* 32: 710-28

Sinninghe Damsté JS. 2016. Spatial heterogeneity of sources of branched tetraethers in shelf systems: The geochemistry of tetraethers in the Berau River delta (Kalimantan, Indonesia). *Geochimica et Cosmochimica Acta* 186: 13-31

Sluijs A, Bijl P, Schouten S, Röhl U, Reichart G-J, Brinkhuis H. 2011. Southern ocean warming, sea level and hydrological change during the Paleocene-Eocene thermal maximum. *Climate of the Past* 7

Sluijs A, Brinkhuis H, Schouten S, Bohaty SM, John CM, et al. 2007. Environmental precursors to rapid light carbon injection at the Palaeocene/Eocene boundary. *Nature* 450: 1218-21

Sluijs A, Frieling J, Inglis GN, Nierop KG, Peterse F, et al. 2020. Late Paleocene–early Eocene Arctic Ocean sea surface temperatures: reassessing biomarker paleothermometry at Lomonosov Ridge. *Climate of the Past* 16: 2381-400

Sluijs A, Schouten S, Pagani M, Woltering M, Brinkhuis H, et al. 2006. Subtropical Arctic Ocean temperatures during the Palaeocene/Eocene thermal maximum. *Nature* 441: 610-3

Sluijs A, van Roij L, Harrington GJ, Schouten S, Sessa JA, et al. 2014. Warming, euxinia and sea level rise during the Paleocene–Eocene Thermal Maximum on the Gulf Coastal Plain: implications for ocean oxygenation and nutrient cycling. *Clim. Past* 10: 1421-39

Smith RW, Bianchi TS, Li X. 2012. A re-evaluation of the use of branched GDGTs as terrestrial biomarkers: Implications for the BIT Index. *Geochimica et Cosmochimica Acta* 80: 14-29

Stokke EW, Jones MT, Tierney JE, Svensen HH, Whiteside JH. 2020. Temperature changes across the Paleocene-Eocene Thermal Maximum–a new high-resolution TEX86 temperature record from the Eastern North Sea Basin. *Earth and Planetary Science Letters* 544: 116388

Taylor KW, Huber M, Hollis CJ, Hernandez-Sanchez MT, Pancost RD. 2013. Re-evaluating modern and Palaeogene GDGT distributions: Implications for SST reconstructions. *Global and Planetary Change* 108: 158-74

Tibbett EJ, Warny S, Tierney JE, Wellner JS, Feakins SJ. 2022. Cenozoic Antarctic Peninsula Temperatures and Glacial Erosion Signals From a Multi- Proxy Biomarker Study. *Paleoceanography and Paleoclimatology* 37: e2022PA004430

Tierney JE, Zhu J, Li M, Ridgwell A, Hakim GJ, et al. 2022. Spatial patterns of climate change across the Paleocene–Eocene Thermal Maximum. *Proceedings of the National Academy of Sciences* 119: e2205326119

Tipple BJ, Pagani M, Krishnan S, Dirghangi SS, Galeotti S, et al. 2011. Coupled high-resolution marine and terrestrial records of carbon and hydrologic cycles variations during the Paleocene–Eocene Thermal Maximum (PETM). *Earth and Planetary Science Letters* 311: 82-92

Uda I, Sugai A, Itoh YH, ITOH T. 2004. Variation in molecular species of core lipids from the order Thermoplasmales strains depends on the growth temperature. *Journal of oleo science* 53: 399-404

Warden L, Kim J-H, Zell C, Vis G-J, de Stigter H, et al. 2016. Examining the provenance of branched GDGTs in the Tagus River drainage basin and its outflow into the Atlantic Ocean over the Holocene to determine their usefulness for paleoclimate applications. *Biogeosciences* 13: 5719-38

Weijers JW, Schouten S, Sluijs A, Brinkhuis H, Damsté JSS. 2007a. Warm arctic continents during the Palaeocene–Eocene thermal maximum. *Earth and Planetary Science Letters* 261: 230-8

Weijers JW, Schouten S, Spaargaren OC, Damsté JSS. 2006. Occurrence and distribution of tetraether membrane lipids in soils: Implications for the use of the TEX86 proxy and the BIT index. *Organic Geochemistry* 37: 1680-93

Weijers JW, Schouten S, van den Donker JC, Hopmans EC, Sinninghe Damsté JS. 2007b. Environmental controls on bacterial tetraether membrane lipid distribution in soils. *Geochimica et Cosmochimica Acta* 71: 703-13

Willard DA, Donders TH, Reichgelt T, Greenwood DR, Sangiorgi F, et al. 2019. Arctic vegetation, temperature, and hydrology during Early Eocene transient global warming events. *Global and Planetary Change* 178: 139-52

Xiao W, Wang Y, Zhou S, Hu L, Yang H, Xu Y. 2016. Ubiquitous production of branched glycerol dialkyl glycerol tetraethers (brGDGTs) in global marine environments: a new source indicator for brGDGTs. *Biogeosciences* 13: 5883-94

Xie S, Liu X-L, Schubotz F, Wakeham SG, Hinrichs K-U. 2014. Distribution of glycerol ether lipids in the oxygen minimum zone of the Eastern Tropical North Pacific Ocean. *Organic Geochemistry* 71: 60-71

Zachos JC, Schouten S, Bohaty S, Quattlebaum T, Sluijs A, et al. 2006. Extreme warming of mid-latitude coastal ocean during the Paleocene-Eocene Thermal Maximum: Inferences from TEX86 and isotope data. *Geology* 34: 737-40

Zell C, Kim J-H, Hollander D, Lorenzoni L, Baker P, et al. 2014a. Sources and distributions of branched and isoprenoid tetraether lipids on the Amazon shelf and fan: Implications for the use of GDGT-based proxies in marine sediments. *Geochimica et Cosmochimica Acta* 139: 293-312

Zell C, Kim J-H, Moreira-Turcq P, Abril G, Hopmans EC, et al. 2013. Disentangling the origins of branched tetraether lipids and crenarchaeol in the lower Amazon River: Implications for GDGT-based proxies. *Limnol. Oceanogr* 58: 343-53

Zell C, Kim JH, Balsinha M, Dorhout D, Fernandes C, et al. 2014b. Transport of branched tetraether lipids from the Tagus River basin to the coastal ocean of the Portuguese margin: consequences for the interpretation of the MBT'/CBT paleothermometer. *Biogeosciences Discuss.* 11: 3731-76

Zhang YG, Pagani M, Wang Z. 2016. Ring Index: A new strategy to evaluate the integrity of TEX86 paleothermometry. *Paleoceanography* 31: 220-32

Zhang YG, Zhang CL, Liu X-L, Li L, Hinrichs K-U, Noakes JE. 2011. Methane Index: a tetraether archaeal lipid biomarker indicator for detecting the instability of marine gas hydrates. *Earth and Planetary Science Letters* 307: 525-34

Figure captions:

Fig. 1: Site map showing the location of the South Dover Bridge core (yellow star). Dashed line represents the border between different US states

Fig. 2. Principal Component Analysis (PCA) of Paleocene-Eocene Thermal Maximum samples at (a) South Dover Bridge, (b) ODP Site 1172, (c) Otaio River, and (d) IODP Site 302 plotted in reduced dimensional space based on the fractional abundance of GDGTs. Black lines represented the loadings of the dominant GDGTs only. Coloured samples represent their assignment determined via the BiGMAC algorithm. The larger symbols represent the average value for a given depositional environment.

Fig. 3: (a) TEX_{86} and (b) MBT_{5ME} values during the Paleocene-Eocene Thermal Maximum at South Dover Bridge. Samples are colour coded based on curated groups.

Fig. 4: Impact of reworking on sea surface temperature estimates during the PETM. a) bulk $\delta^{18}O$ carbonate values (Lyons et al,. 2019), b) TEX_{86} values (*this study*), c) TEX_{86}-derived SST estimates calculated using the BAYSPAR calibration (Tierney and Tingley, 2015), d) BIT values, where high values indicate enhanced input of organic carbon derived from (pre-aged) soil and/or peat (*this study*), e) Terrestrial-aquatic ratio (TAR), where high values indicate enhanced input of organic carbon from terrestrial higher plants (Lyons et al., 2019), and f) f_{fossil}, the fraction of organic carbon derived from thermally mature fossil sources (Lyons et al., 2019)

Fig. 5: Impact of reworking on mean annual air temperature estimates during the PETM. a) bulk $\delta^{18}O$ carbonate values (Lyons et al,. 2019), b) MBT_{5ME} values (*this study*), c) MBT_{5ME}-derived MAAT estimates calculated using the BAYMBT calibration (Crampton-Flood et al., 2020) (*this study*), d) BIT index, where high values indicating input of (pre-aged) soil and/or peat organic matter (*this study*), e) $\#rings_{tetra}$, where high values indicate a greater proportion of brGDGTs derived from marine in-situ production (*this study*), and f) the Isomerisation Ratio (IR), where high values indicate a greater proportion of brGDGTs derived from rivers and/or alkaline soils (Lyons et al., 2019) (*this study*).

Fig. 6: High-resolution, multi-proxy reconstructions of sea surface temperature (SST) during the Paleocene-Eocene Thermal Maximum (PETM) at South Dover Bridge. a) Bulk $\delta^{18}O$ carbonate values (Lyons et al,. 2019), b) TEX_{86}-derived SST estimates calculated using the BAYSPAR calibration (Tierney and Tingley, 2015), and c-e) pH-corrected, Mg/Ca-derived SST estimates from (c-d) surface-dwelling photosymbiont-bearing *Acarinina* and *Morozovella* spp., and (e) deeper-dwelling *Subbotina* spp. (Babila et al,. 2022).

Highlights:

- We assess the impact of organic carbon reworking on GDGT proxies during the PETM
- TEX_{86} values are unaffected by reworking and can be used to reconstruct SSTs
- MBT_{5ME} values can be highly variable and affected by multiple secondary inputs
- Discerning the provenance of GDGTs in coastal settings is crucial for related proxies

Keywords: GDGTs, biomarkers, hyperthermals, reworking

Figure 1

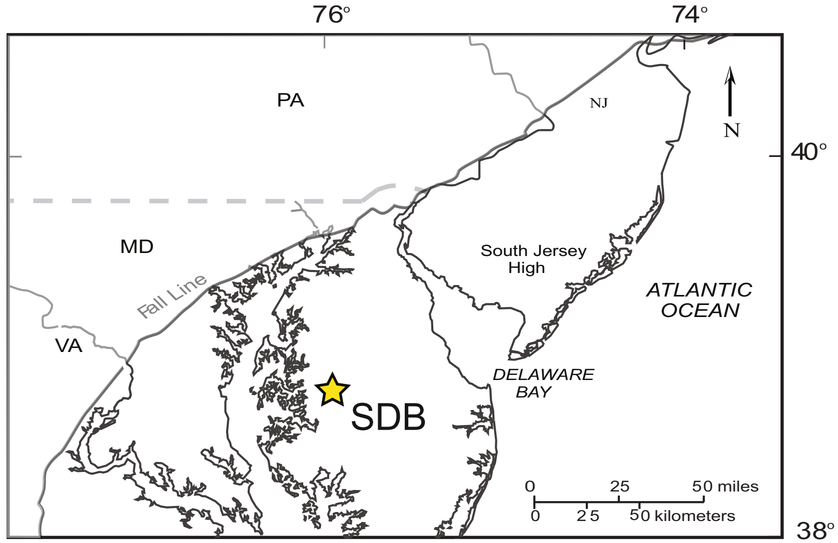
76°
74°
40°
38°
PA
NJ
N
MD
VA
Fall Line
South Jersey
High
ATLANTIC
OCEAN
DELAWARE
BAY
SDB
0
25
50 miles
0
25
50 kilometers

Figure 2

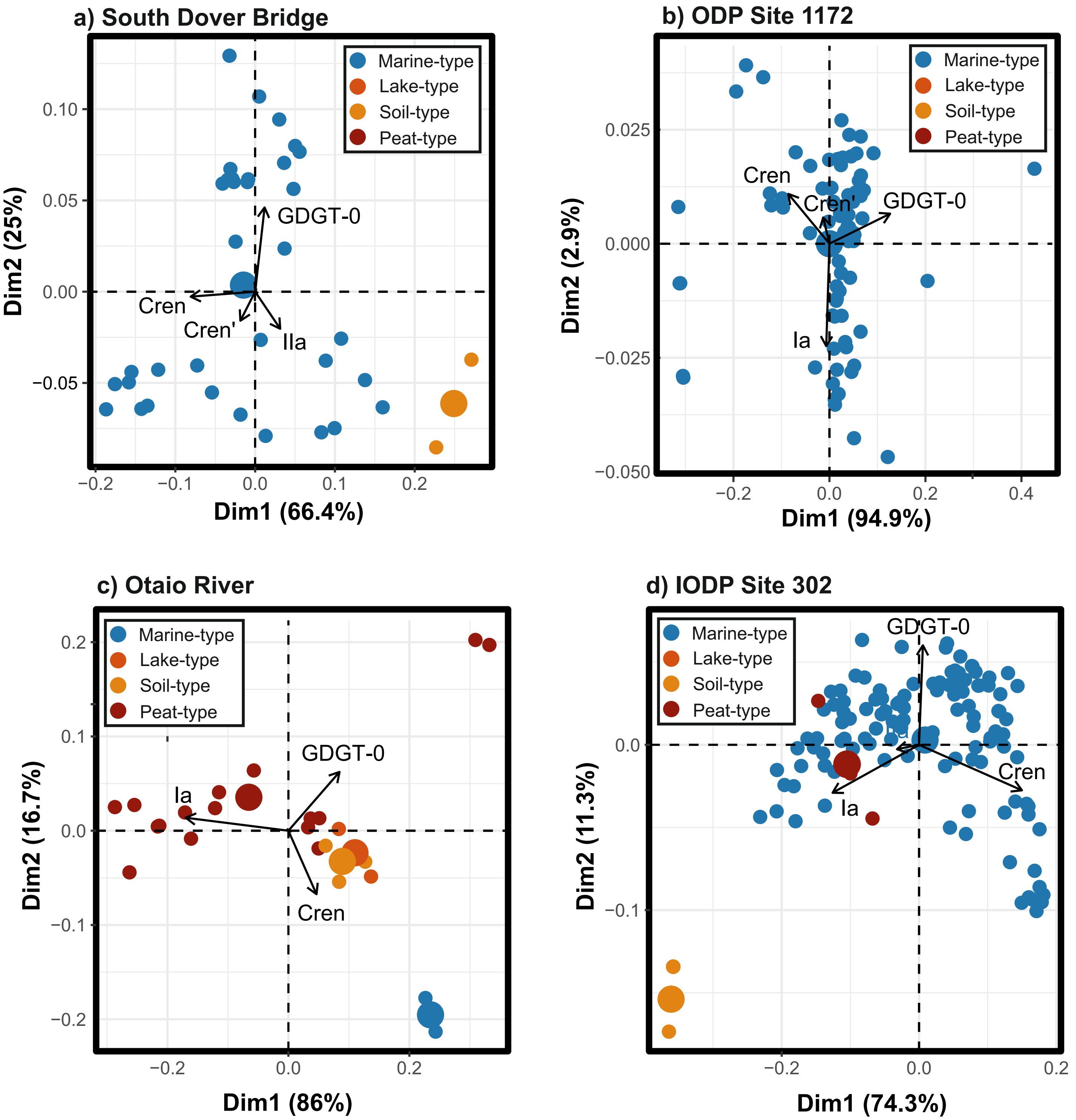

a) South Dover Bridge
Marine-type
Lake-type
Soil-type
Peat-type
GDGT-0
Cren
Cren'
IIa
Dim1 (66.4%)
Dim2 (25%)
b) ODP Site 1172
Marine-type
Lake-type
Soil-type
Peat-type
Cren
Cren'
GDGT-0
Ia
Dim1 (94.9%)
Dim2 (2.9%)
c) Otaio River
Marine-type
Lake-type
Soil-type
Peat-type
GDGT-0
Ia
Cren
Dim1 (86%)
Dim2 (16.7%)
d) IODP Site 302
Marine-type
Lake-type
Soil-type
Peat-type
GDGT-0
Cren
Ia
Dim1 (74.3%)
Dim2 (11.3%)

Figure 3

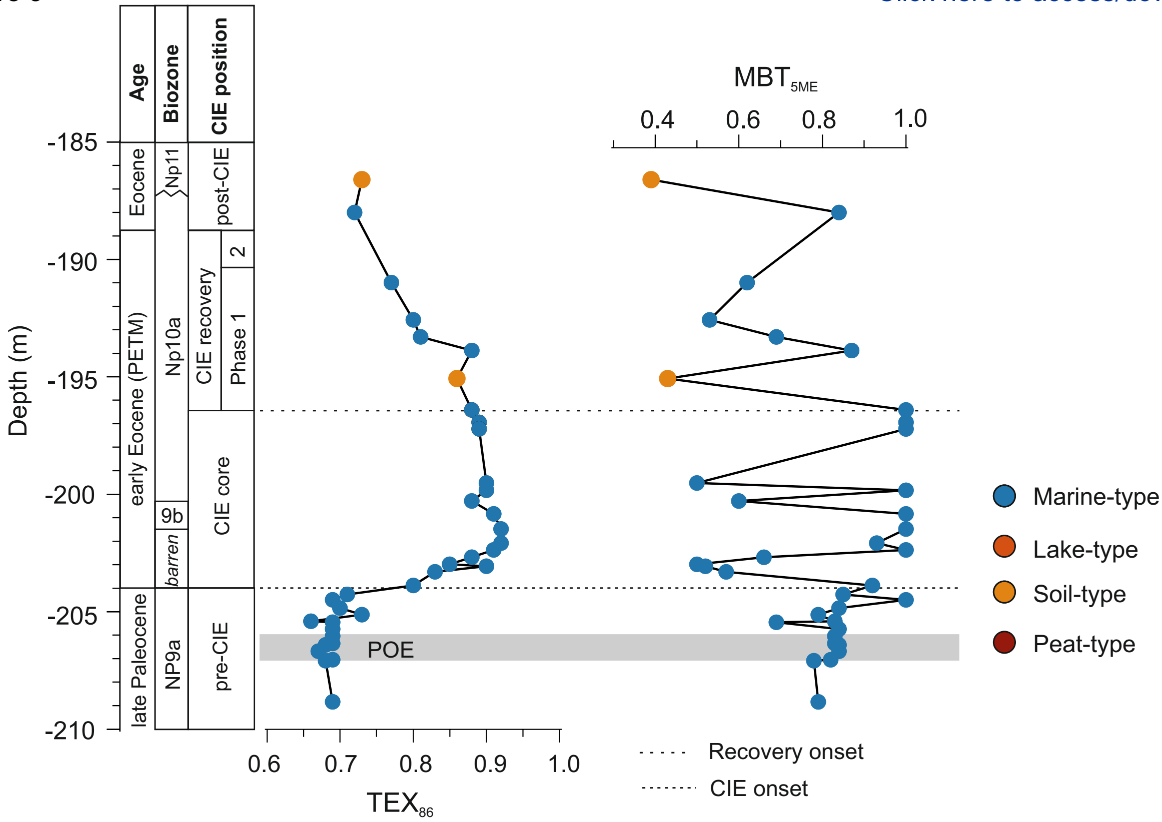

Age
Biozone
CIE position
Depth (m)
-185
-190
-195
-200
-205
-210
Eocene
early Eocene (PETM)
late Paleocene
Np11
Np10a
9b
barren
NP9a
post-CIE
CIE recovery
2
Phase 1
CIE core
pre-CIE
POE
TEX86
0.6
0.7
0.8
0.9
1.0
MBT5ME
0.4
0.6
0.8
1.0
Recovery onset
CIE onset
Marine-type
Lake-type
Soil-type
Peat-type

Figure 4

Click here to access/download;Figure;Figure 4.pdf

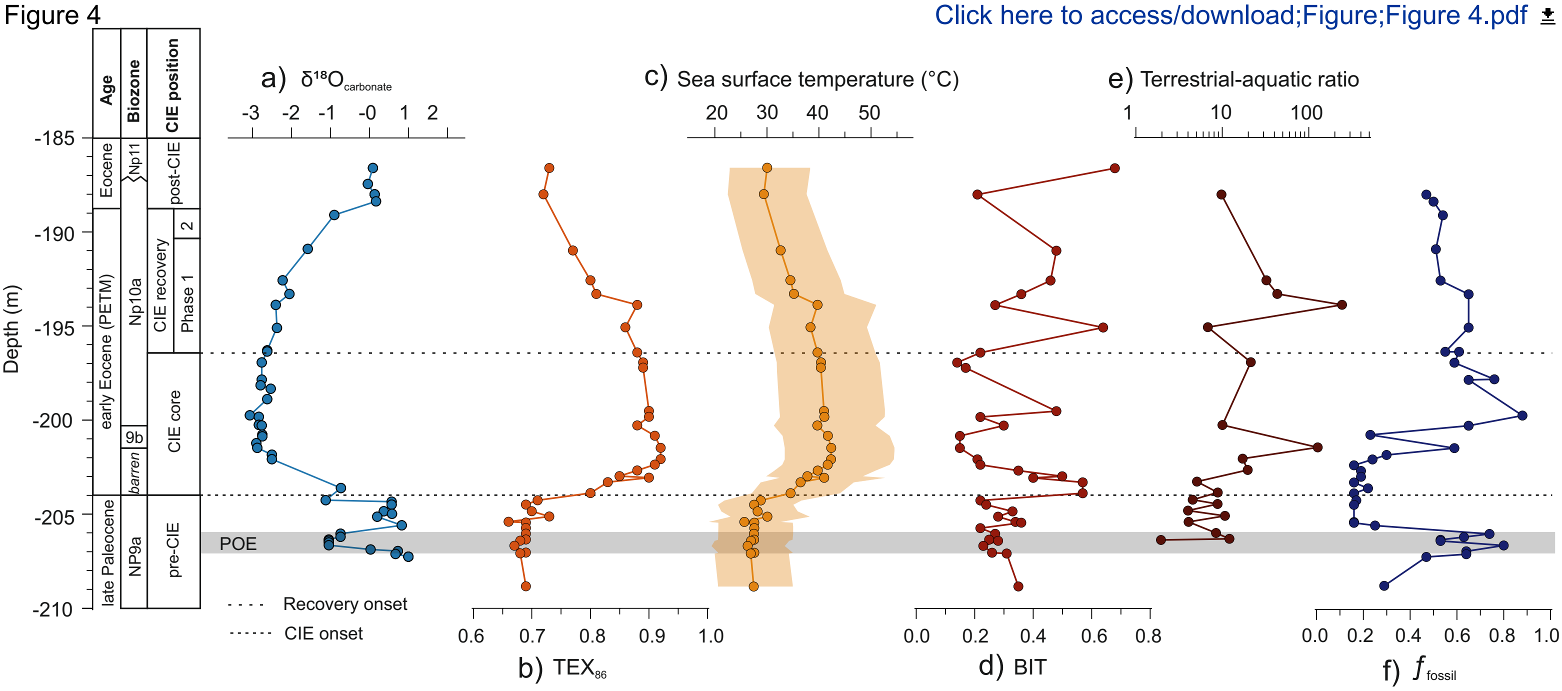

Figure 5

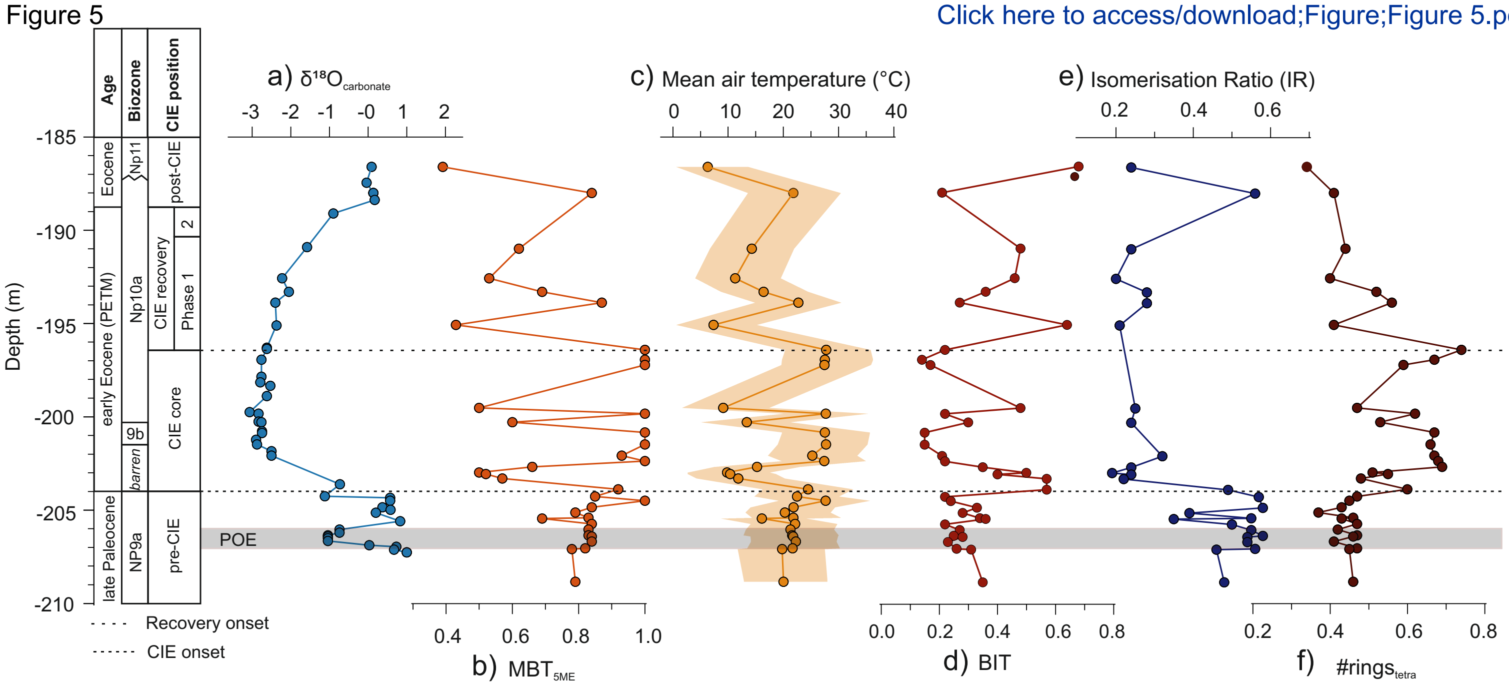
Age
Biozone
CIE position
Depth (m)
a) δ18O carbonate
c) Mean air temperature (°C)
e) Isomerisation Ratio (IR)
Eocene
early Eocene (PETM)
late Paleocene
Np11
Np10a
9b
barren
NP9a
post-CIE
CIE recovery
Phase 1
2
CIE core
pre-CIE
POE
Recovery onset
CIE onset
b) MBT5ME
d) BIT
f) #rings tetra

Figure 6

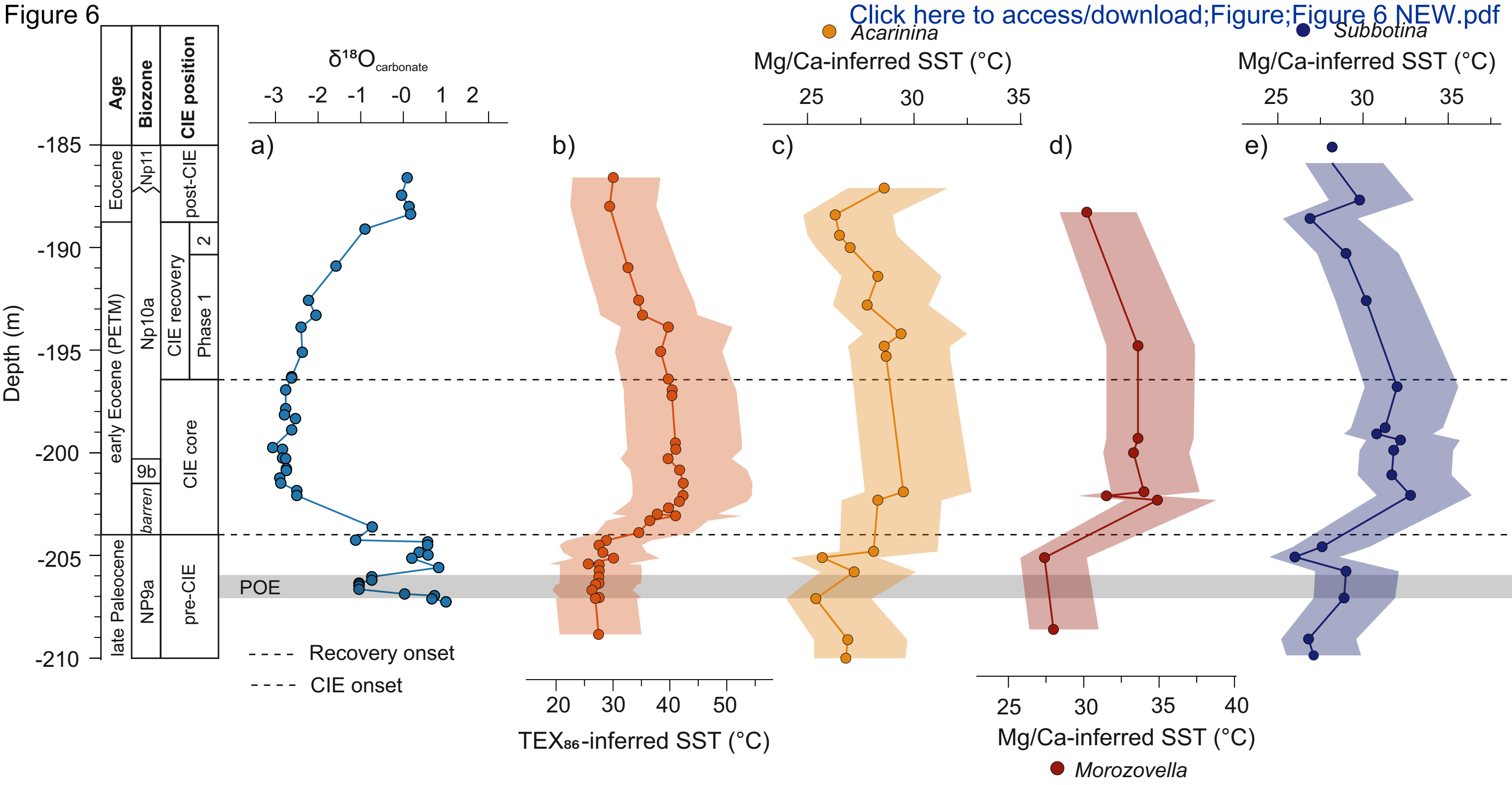
Age
Biozone
CIE position
Eocene
early Eocene (PETM)
late Paleocene
Np11
Np10a
9b
barren
NP9a
post-CIE
CIE recovery
2
Phase 1
CIE core
pre-CIE
Depth (m)
-185
-190
-195
-200
-205
-210
δ18O carbonate
-3
-2
-1
-0
1
2
a)
b)
c)
d)
e)
POE
Recovery onset
CIE onset
20
30
40
50
TEX86-inferred SST (°C)
Acarinina
Mg/Ca-inferred SST (°C)
25
30
35
Morozovella
Mg/Ca-inferred SST (°C)
25
30
35
40
Subbotina
Mg/Ca-inferred SST (°C)
25
30
35